Metals **2015**, *5*, 1746-1769; doi:10.3390/met5031746

OPEN ACCESS

metals

ISSN 2075-4701

www.mdpi.com/journal/metals/

Article

Experimental Study of the Mg-Ni-Y System at 673 K Using Diffusion Couples and Key Alloys

Mohammad Mezbahul-Islam [1], Dmytro Kevorkov [1] and Mamoun Medraj [1,2,*]

[1] Department of Mechanical and Industrial Engineering, Concordia University, 1455 de Maisonneuve Blvd. West, Montreal, QC H3G 1M8, Canada; E-Mails: mezbahul@gmail.com (M.M.-I.); kevorkov@encs.concordia.ca (D.K.)

[2] Mechanical and Materials Engineering, Masdar Institute, P.O. Box 54224, Abu Dhabi, UAE

***** Author to whom correspondence should be addressed; E-Mail: mmedraj@encs.concordia.ca; Tel.: +1-514-848-2424 (ext. 3146); Fax: +1-514-848-3175.

Academic Editor: Hugo F. Lopez

Received: 1 September 2015 / Accepted: 16 September 2015/ Published: 22 September 2015

Abstract: Three solid-solid and two solid-liquid diffusion couples together with 32 key samples were used to construct the isothermal section of the Mg-Ni-Y system at 673 K. The present investigation revealed 12 ternary intermetallic compounds. Crystal structures of two ternary compounds τ_1 (Gd_4RhIn prototype with lattice parameter of a = 1.3666 nm) and τ_2 (Mo_2FeB_2 prototype with lattice parameters of a = 0.7395 nm and c = 0.3736 nm) were determined. The phase relations and ternary solubility of the binary and ternary compounds at 673 K were determined using scanning electron microscopy (SEM), wave dispersive X-ray spectrometer (WDS) and X-ray diffraction (XRD) analysis.

Keywords: phase equilibrium; isothermal section; diffusion couple; crystallography; Rietveld refinement

---

1. Introduction

Mg-based alloys are widely used in structural applications because of their high strength to weight ratio. Light weight alloys reduce the fuel consumption of automobiles. The innovation and rapid development of Mg-based metallic glass can further improve the physical and chemical properties of these alloys. It has been found that amorphization to produce metallic glass by a higher cooling rate

improves the mechanical strength, hardness and corrosion resistance compared to the crystalline alloys [1–5]. Some of the promising metallic glasses with large super cooled liquid region have been reported in the Mg-Ni-Y system [1,6]. In addition to structural applications, Mg-Ni-Y alloys have been used for hydrogen storage purpose [7]. Mg_2Ni has been used commercially as hydrogen storage material. It is found that addition of Y to Mg_2Ni improves the rate and amount of hydrogen absorption [7]. It is also found that amorphization increases the hydrogen storage capacity of the crystalline alloys [8,9] due to their short-range order structures and extra free volume. This enhances the diffusion and site occupation of the hydrogen atoms in the amorphous matrix [10]. It is possible to have new metallic glass alloys suitable for hydrogen storage application in the Mg-Ni-Y system. Thus a clear understanding of the phase equilibrium in the Mg-Ni-Y system is required.

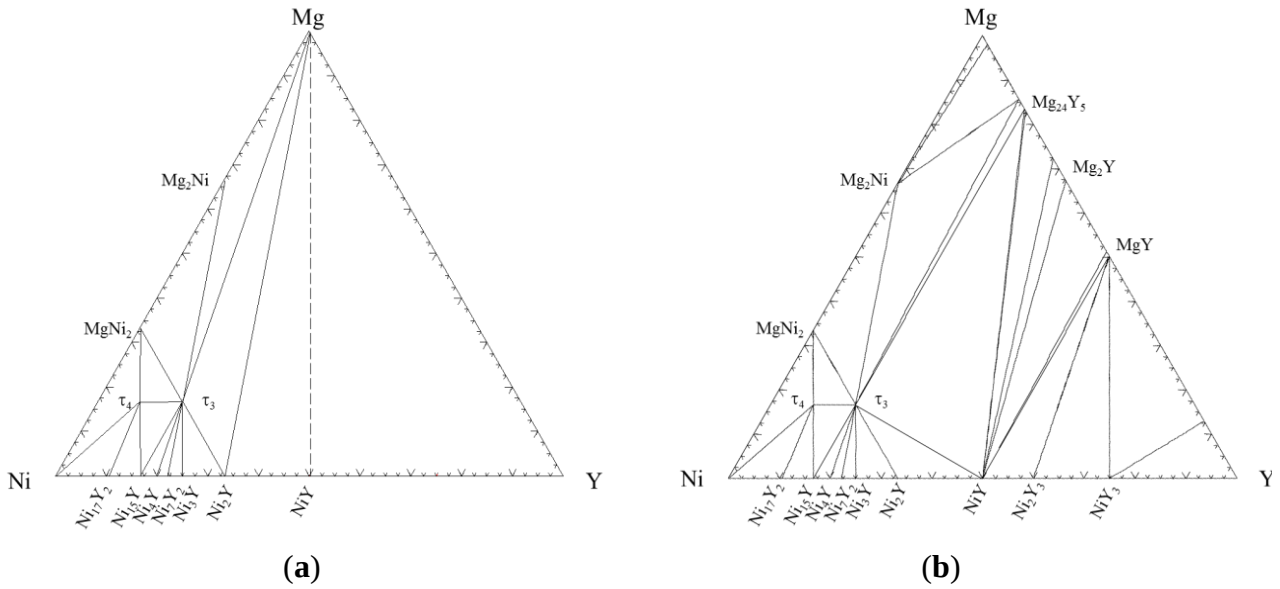

Figure 1. (**a**) Isothermal section of the Mg-Ni-Y system at 673 K (Ni-rich part) [11]; (**b**) Calculated isothermal section of the Mg-Ni-Y system at 673 K [16].

Limited amount of experimental work has been done on this system. Yao *et al.* [11] investigated the 673 K isothermal section of the Ni-rich region using X-ray diffraction (XRD), scanning electron microscopy (SEM), and differential thermal analysis (DTA) and reported a partial section as shown in Figure 1a. They [11] confirmed the occurrence of two ternary compounds τ_3 ($MgNi_4Y$) and τ_4 (Mg_2Ni_9Y). The compositions of these ternary compounds were reported earlier by Kadir *et al.* [12–14] and Aona *et al.* [15]. Mezbahul-Islam and Medraj [16] thermodynamically optimized the system based on the available experimental data until 2009 as shown Figure 1b. Later the same authors [17] published a partial isothermal section along the Mg-NiY line at 673 K. They [17] reported the presence of five new ternary compounds, τ_2 ($Mg_3Ni_2Y_4$), τ_5 ($MgNi_2Y_2$), τ_6 (MgNiY), τ_{10} (Mg_5NiY), and τ_{11} ($Mg_{8-13}NiY$) based on key sample analysis. Recently, Wang *et al.* [18] reported two isothermal sections with less than 50 at% Y at 673 and 773 K. The experimental investigation of Wang *et al.* [18] confirmed the presence of three ternary compounds, τ_3 ($MgNi_4Y$), τ_4 (Mg_2Ni_9Y) and τ_5 ($MgNi_2Y_2$). Another investigation by Jiang *et al.* [19] proved the existence of a Mg-rich ternary compound τ_{11} ($Mg_{91}Ni_4Y_5$). However, complete understanding of the phase relations across the whole

compositional range is still unknown. It can be seen in the previous works that either the Ni-rich or the Mg-rich side of the Mg-Ni-Y system had been experimentally investigated. However, other ternary compounds may still exist which will make the phase relations significantly different in this system. The chemistry of the phases and their structural details should be further studied. Therefore, it was decided to investigate the system experimentally in order to have better understanding of the phase equilibria for the whole composition range.

2. Experimental Procedure

In order to establish the phase relations, three solid-solid and two solid-liquid diffusion couples together with 32 key samples were utilized. The actual composition of the key alloys along with the terminal composition of the diffusion couples' end-members are shown in Figure 2. The diffusion couple is a powerful and efficient technique for mapping the phase diagram of ternary systems [20–22]. It also eliminates the problems associated with alloy preparation especially for the systems with high melting temperatures [23]. Within the diffusion layers the equilibrium phases occur, whereas at the interface local equilibrium takes place [23]. However, one should always consider the possibility of missing phases [23,24] while using the diffusion couple for determining the phase diagram. This may occur because of the slow nucleation of the phase which prevents formation of the diffusion layer. In order to obtain more reliable information, Kodentsov *et al.* [23], among others, suggested to combine the diffusion couple method with key sample analysis. Therefore, in the present work both of these techniques were used.

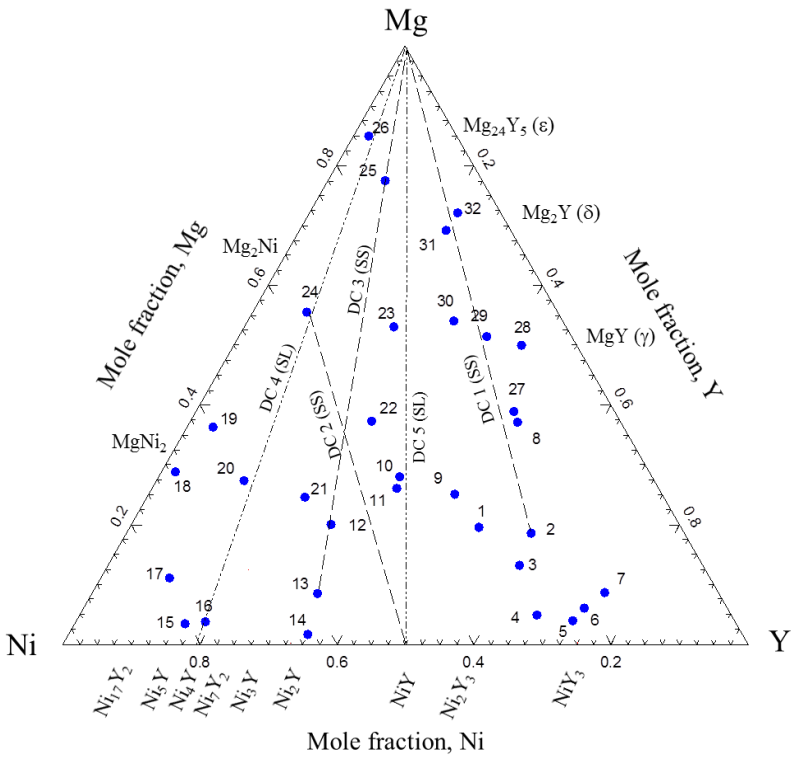

Figure 2. Actual global composition of the Mg-Ni-Y alloys. Dotted lines show the diffusion couples. SS and SL refer to the solid-solid and solid-liquid diffusion couples.

The key alloys were prepared using an arc melting furnace equipped with a water cooled copper crucible under flowing argon. The purity of the elements used was Cu–99.99%, Ni–99.99%, and Y–99.9%, all supplied by Alfa Aesar (Haverhill, MA, USA). The furnace chamber was evacuated and purged by argon several times before melting. Each alloy was crushed and remelted at least four times to ensure homogeneity. The actual global composition of the samples was identified by Inductively Coupled Plasma-Optical Emission Spectrometry (ICP-OES) (Ultima-2 ICP from Horiba Scientific, Edison, NJ, USA). The solid-solid diffusion couples were prepared from two end-member blocks of pure Mg, binary or ternary alloys. Contacting surfaces of these blocks were pre-grinded down to 1200 grit using SiC paper and polished with 1 μm diamond paste and 99% ethanol as a lubricant. The blocks were pressed together using clamping rings, placed in a Ta container and sealed in a quartz tube under protective Ar atmosphere. The key alloys and diffusion couples were annealed at 673 K for 4 weeks. Although a higher annealing temperature is desirable for faster kinetics, this temperature should be chosen below the lowest melting point in the system to avoid melting during annealing. In the present work, the annealing temperature was chosen based on the lowest eutectic of the three pertinent binary systems. Among the three binaries the lowest eutectic occurs in the Mg-Ni system at around 782 K. Therefore, it was decided to anneal the samples at 673 K to reach equilibrium faster without melting. These alloys were then characterized by light optical microscopy, scanning electron microscopy (SEM) and wave dispersive X-ray spectrometer (WDS) using point and line scans. The Hitachi (Tokyo, Japan) S-3400N SEM equipped with WDS and EDS Oxford® (Abingdon, UK) detectors was used for the elemental analysis. The error of the WDS measurements was estimated to be around ±1 at%. The XRD patterns were obtained using a PANanalytical Xpert Pro powder X-ray diffractometer (Almelo, The Netherlands) with a CuKα radiation. The XRD spectrum was acquired from 20 °to 120 °2θ with a 0.02 °step size. XRD analysis of the samples was carried out using X'Pert HighScore Plus Rietveld analysis software (Almelo, The Netherlands).

3. Results and Discussion

3.1. Diffusion Couple Analysis

3.1.1. Solid-Solid Diffusion Couple 1

Backscatter electron (BSE) images of the solid-solid diffusion couple 1 are shown in Figure 3. This diffusion couple is between Mg and sample 20 (18.5/22.4/59.1 Mg/Ni/Y at%) as shown in Figure 2. The ternary alloy consists of three phases: NiY, τ_1 ($MgNiY_4$) and τ_5 ($Mg_{29}Ni_{20}Y_{42}$). These end members were chosen in order to identify the intermetallic compounds located in the Mg-Y side of the Gibbs triangle. The diffusion couple was annealed for four weeks at 673 K. During the heat treatment, extensive interdiffusion among Mg, Ni, and Y took place allowing various equilibrium phases to form. Each layer represents a phase which is in equilibrium with its adjacent layers. The microstructure of the diffusion couple with increased magnification of the area of interest is shown in Figure 3b. The compositions of the formed phases were detected by the WDS point analysis. The WDS line scans were used to determine the solubility ranges and phase equilibria among the intermetallics. The same approach was used to study other diffusion couples.

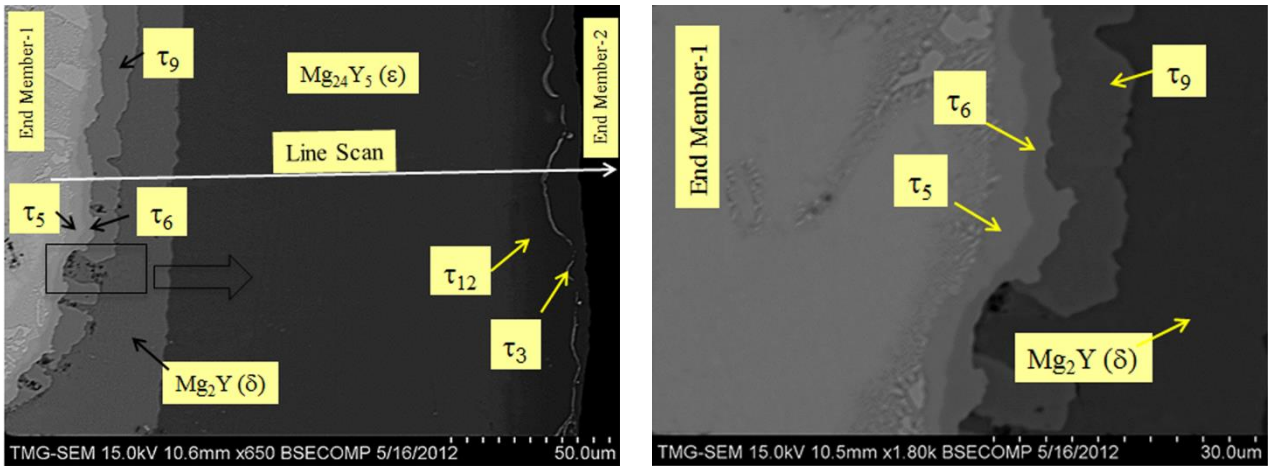

(**a**) (**b**)

Figure 3. (**a**) Solid-solid diffusion couple of Mg–sample 20 (18.5/22.4/59.1 Mg/Ni/Y at%) annealed at 673 K for 4 weeks; (**b**) Magnified area of interest.

The diffusion path through the entire system is shown in Figure 4a. The composition profile as shown in Figure 4b explains the configuration of these layers and has been used to distinguish each layer. By taking advantage of the local equilibrium at the interfaces formed between the layers, the sequence of phases along the diffusion path can be deduced as:

{NiY + τ_1 + τ_5} (end-member 1) → τ_5 → τ_6 → τ_9 → $Mg_2Y(\delta)$ → $Mg_{24}Y_5(\varepsilon)$ → τ_{12} → {hcp-Mg} (end-member 2).

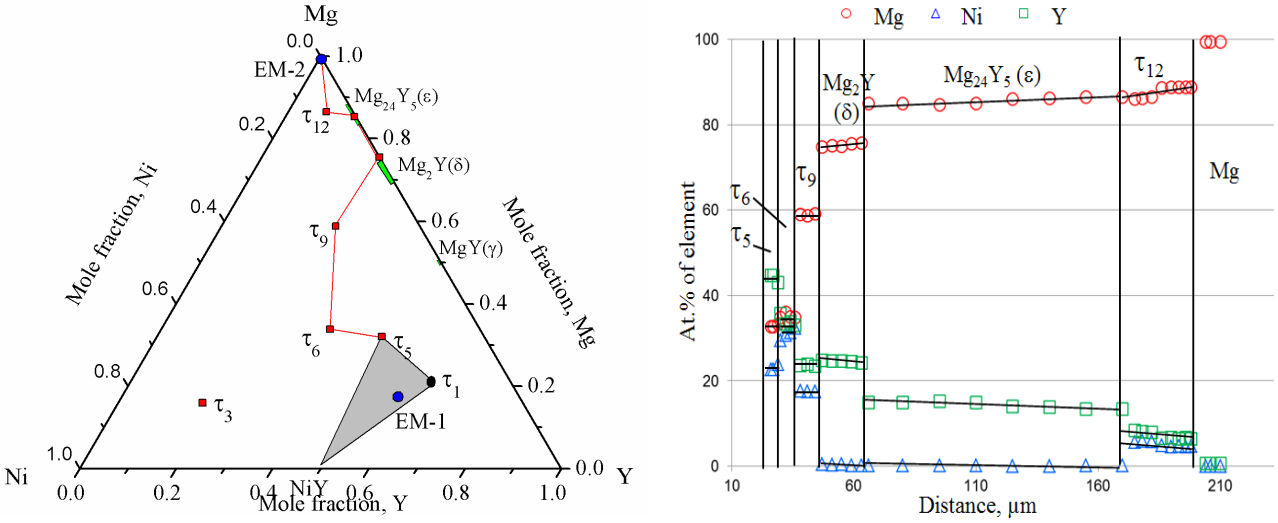

(**a**) (**b**)

Figure 4. (**a**) Diffusion path projected on the Mg-Ni-Y Gibbs triangle; (**b**) Composition profile of the diffusion couple 1 along the line scan shown in Figure 3.

The first diffusion layer was found to have a composition of $Mg_{32.9}Ni_{22.5}Y_{44.6}$. According to the SEM/WDS analysis this layer was identified as a ternary compound, τ_5 ($Mg_{29}Ni_{20}Y_{42}$). The layer is thin (~4 μm), but can be seen clearly at higher magnification in Figure 3b. After that the diffusion path reaches the second layer with a composition of $Mg_{35.4}Ni_{31.5}Y_{33.1}$, which is also a ternary compound, τ_6.

The layer is about 5 μm in width. The composition of this layer indicates a ternary compound of almost equal amount of each element suggesting the MgNiY formula. The next diffusion layer represents τ_9 ($Mg_{57}Ni_{18}Y_{25}$), which is another ternary compound with approximate composition of $Mg_{59.1}Ni_{16.5}Y_{24.4}$. These three intermetallics, τ_5, τ_6, and τ_9 are considered as stoichiometric ternary compounds as the compositional profile in Figure 4b does not show any evidence for significant atomic replacement. Also, considering local equilibrium at the interfaces, τ_5 is in equilibrium with τ_6 and τ_5 is in equilibrium with τ_9. The next diffusion layer represents $Mg_2Y(\delta)$. The width of this layer is about 30 μm. After $Mg_2Y(\delta)$, a large layer of about 90 μm width which was identified as $Mg_{24}Y_5(\varepsilon)$ forms. Ni solubility in both $Mg_2Y(\delta)$ and $Mg_{24}Y_5(\varepsilon)$ was found to be very small (~0.5 at%) which can be considered negligible because it is smaller than the measurement error (±1 at%). However, the maximum Ni solubility could not be confirmed using this diffusion couple as the diffusion path crossed both $Mg_2Y(\delta)$ and $Mg_{24}Y_5(\varepsilon)$ laterally. The maximum solubility of Ni in these compounds was confirmed using key samples as is discussed in Section 3.2. The homogeneity range of $Mg_2Y(\delta)$ and $Mg_{24}Y_5(\varepsilon)$ in the Mg-Y binary is about 70.5–75.8 and 84.2–88.1 at% Mg respectively, at 673 K [25,26]. In this diffusion couple, the solubility was found as 74.8–75.6 and 85–86.3 at% Mg for $Mg_2Y(\delta)$ and $Mg_{24}Y_5(\varepsilon)$, respectively which are within the reported solubility [25,26]. The next diffusion layer represents τ_{12} ($Mg_{15}NiY$) with a composition of $Mg_{86.8}Ni_{5.5}Y_{7.7}$. The composition profile of this layer in Figure 4b shows variation of Mg content from ~86.3 at% to ~89.0 at%, which demonstrates the homogeneity range of τ_{12}. The concentration of Ni and Y changes from ~4.6 to 5.9 at% Ni and ~6.7 to 8.1 at% Y. A very thin white layer can be seen in Figure 3a. WDS analysis of this thin layer revealed a composition that represents τ_3 ($MgNi_4Y$) which was reported earlier [14]. This indicates equilibrium relationship between τ_{12} and τ_3. However this layer could not be shown in Figure 4b because it is very thin. The diameter of the WDS probe is 2 μm which is larger than this layers' thickness. The phase relation: $\tau_{12} + \tau_3$ was confirmed by key samples as is discussed later.

3.1.2. Solid-Solid Diffusion Couple 2

The second solid-solid diffusion couple was used to identify and understand the ternary compounds in the Mg-Ni side of the Mg-Ni-Y system. The two end members have the compositions of 6.2/64.9/28.9 and 55.5/36.6/7.9 Mg/Ni/Y at%. End member 1 is in a two phase region consisting of NiY (0.7/50.3/49.0 Mg/Ni/Y at%) and τ_3 (7.1/66.4/26.5 Mg/Ni/Y at%), whereas end member 2 is located in a three phase region of τ_3 (19.2/65.5/15.3 Mg/Ni/Y at%), Mg_2Ni (66.8/31.4/1.8 Mg/Ni/Y at%) and τ_{12} (91.4.1/4.2/4.4 Mg/Ni/Y at%). These end members were selected to obtain the maximum amount of information. They contain a common phase τ_3 which dominates in this part of the phase diagram. In diffusion couple 1 shown in Figure 3a, a thin layer with a composition similar to τ_3 was observed within the τ_{12} phase. It reflects that τ_3 is in equilibrium with τ_{12}. Due to the locations of τ_3 and τ_{12} (shown in Figure 4), it is possible that τ_3 will have an equilibrium relation with each ternary compound located on the Mg-NiY line. Therefore, a successful diffusion couple with these end members will not only provide information about the presence of any new compounds but will also establish the phase relationship in this region.

The BSE image of the diffusion zone can be seen in Figure 5. It was very difficult to obtain a better diffusion layer due to the formation of a crack during the heat treatment. Only localized diffusion

could be obtained which is analyzed here to extract information of the phase relationship. Five diffusion layers were identified and a line scan through these layers is shown in Figure 6a. Based on the WDS analysis, the diffusion path was estimated as projected on the Gibbs triangle in Figure 6b. The dotted line in Figure 6b shows the tentative phase relations of NiY-τ_6 and τ_6-τ_8 as the diffusion couple did not form τ_6. However, these phase relationships were proven later by the key samples. The diffusion starts with the formation of a white bush shape layer which was identified as NiY. The next layer is about 15 µm thick and was identified as a stoichiometric ternary compound, τ_8 (Mg_2NiY) with of 51.0/24.7/24.2 Mg/Ni/Y at% composition. The next layer is quite thin and is about 6 µm. According to the WDS analysis, its composition is 74.7/12.9/12.4 Mg/Ni/Y at%. It represents another ternary compound, τ_{10} (Mg_6NiY). The subsequent layer is τ_{11} (Mg_9NiY). This layer is about 20 µm thick. The compositional profile in Figure 6a shows a concentration gradient for this compound. The Mg concentration increased from 82.3 at% to 84.1 at%. Whereas, the variation of Ni and Y concentration was found from 7.9–7.1 at% Ni and 9.8–8.7 at% Y. This suggests the presence of the solubility for τ_{11} where Mg has been replaced by Ni and Y. After this layer, the diffusion ends in the three-phase region (Mg_2Ni + τ_{12} + τ_3) of end member 2. The BSE image of the diffusion zone in Figure 5, shows that τ_3 is in contact with all the diffusion layers. This demonstrates that τ_3 has an equilibrium phase relation with each compound on the Mg-NiY line. Some of the phase triangulations are confirmed using the key samples.

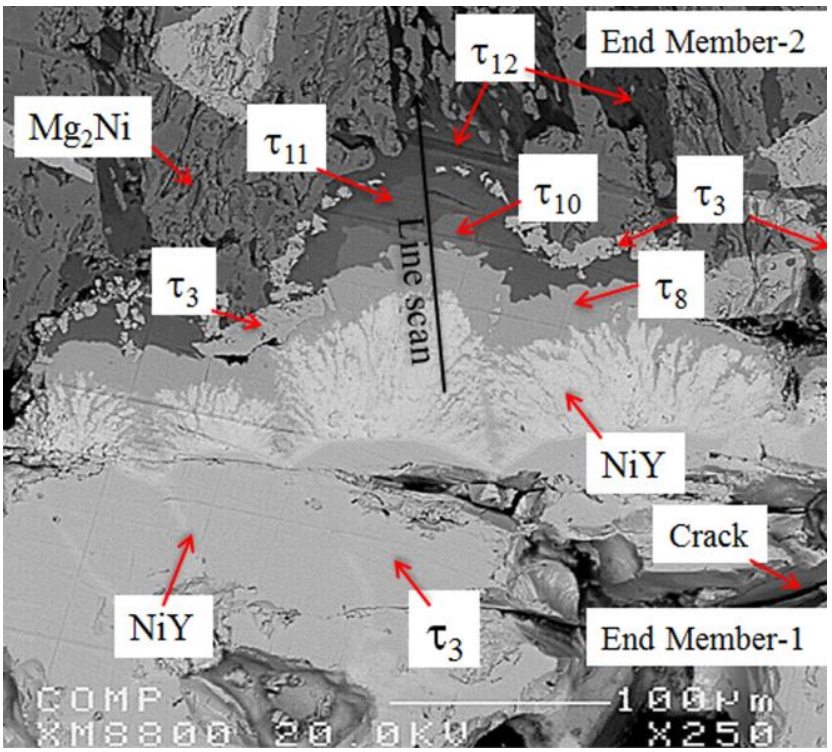

Figure 5. Backscatter electron (BSE) images of the solid–solid diffusion couple 2 annealed at 673 K for 4 weeks.

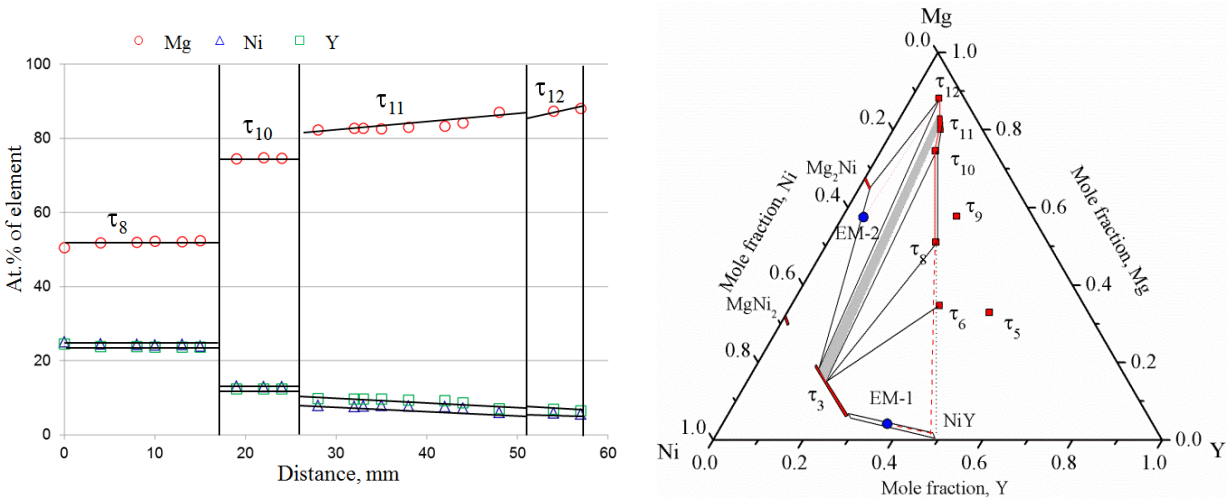

Figure 6. (**a**) Composition profile of the diffusion couple 2 along the line scan shown in Figure 5; (**b**) Extracted phase equilibria based on the solid-solid diffusion couple 2 projected on the Mg-Ni-Y Gibbs triangle. Dotted line indicates expected phase equilibria which is not recognized in DC 2.

3.1.3. Solid-Solid Diffusion Couple 3

The third solid-solid diffusion couple was prepared to confirm some of the ternary compounds already identified in the first two diffusion couples. End members of this diffusion couple are Mg and a ternary alloy with the composition 6.2/64.9/28.9 Mg/Ni/Y at%. This alloy is located in the two-phase region of NiY and τ_3. The BSE image of the diffusion couple is shown in Figure 7a,b with increased magnification.

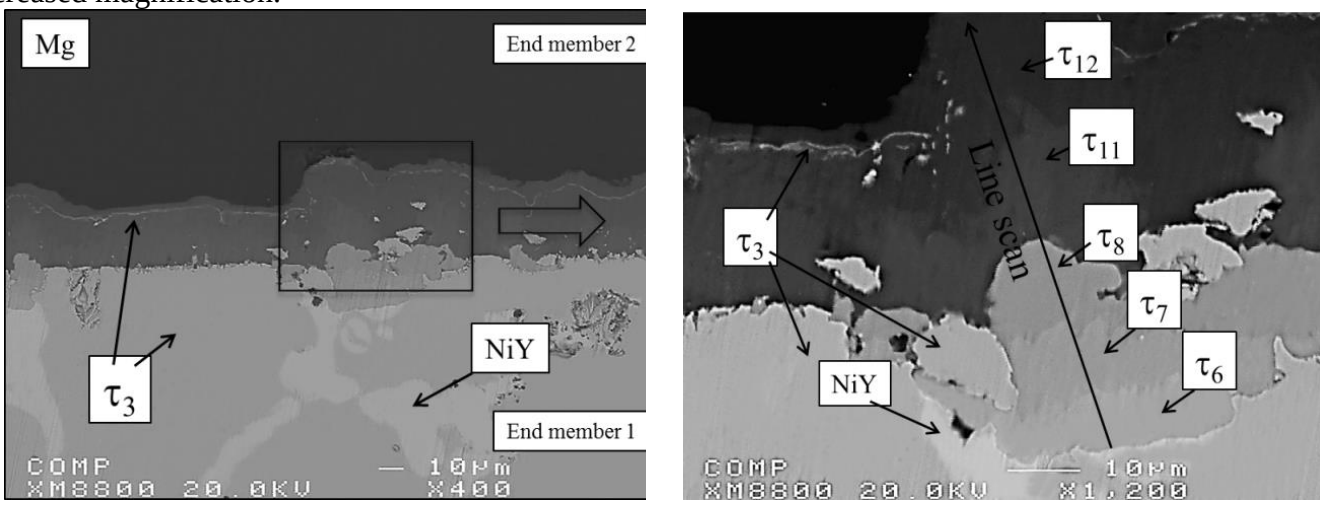

Figure 7. (**a**) BSE images of the solid-solid diffusion couple-3 annealed at 673 K for 4 weeks; (**b**) Magnified area of interest.

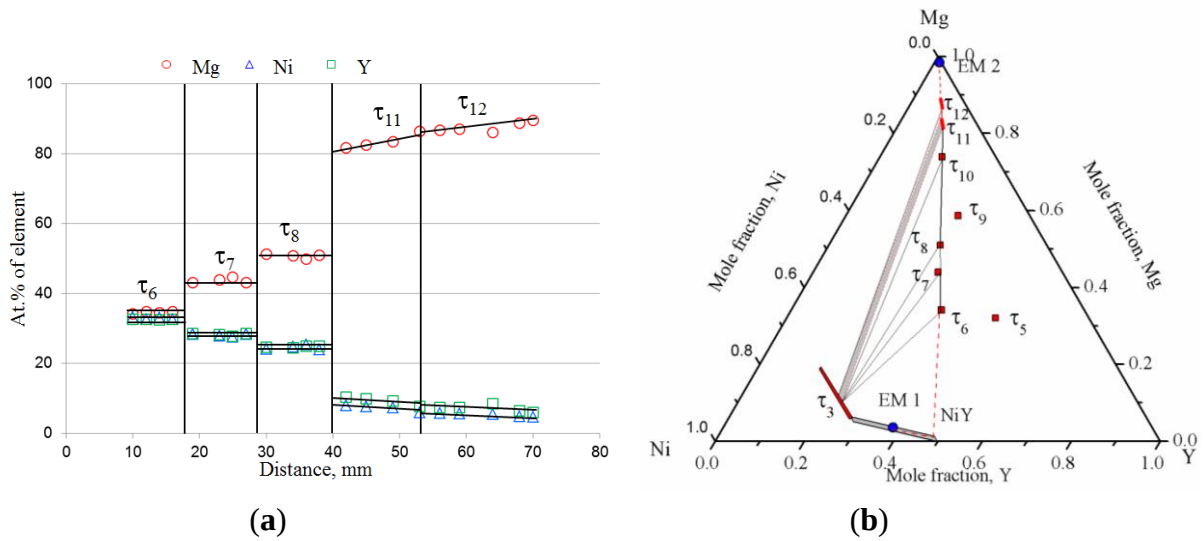

(**a**) (**b**)

Figure 8. (**a**) Composition profile along the line scan shown in Figure 7b; (**b**) Extracted phase equilibria based on the solid-solid diffusion couple 3 projected on the Mg-Ni-Y Gibbs triangle. Dotted lines indicate expected phase equilibria which are not recognized in DC 3.

The BSE image in Figure 7b shows the formation of a small region with five diffusion layers. In order to identify them properly, a WDS line scan was performed. The composition profile as a result of the line-scan has been shown in Figure 8a. It reveals five ternary compounds. These compounds are τ_6 (MgNiY), τ_7 ($Mg_8Ni_5Y_5$), τ_8 (Mg_2NiY), τ_{11} (Mg_xNiY, $x \cong 9$–13), and τ_{12} (Mg_xNiY, $x \cong 13$–18). Except τ_7 ($Mg_8Ni_5Y_5$), other ternary compounds were identified in the previous two diffusion couples. The phase relations confirmed from this diffusion couple are: {NiY + τ_3} (end-member 1)/τ_3 + τ_6 + τ_7/τ_3 + τ_7 + τ_8/τ_3 + τ_{11} + τ_{12}/τ_3 + τ_{12}/{τ_{12} + hcp-Mg} (end-member 2). τ_{11} (81.7–83.5 at% Mg, 7.9–7.3 at% Ni, 10.4–9.2 at% Y) and τ_{12} (86.3–89.5 at% Mg, 6.0–4.6 at% Ni, 7.7–5.9 at% Y) show some solubility as can be seen in the composition profile in Figure 8a. Both of these compounds show similar type of solubility where Mg has been replaced by an almost equal amount of Ni and Y. The phase relations obtained based on the solid-solid diffusion couple 3 are shown in Figure 8b. The ternary compounds identified in all the three solid-solid diffusion couples are shown with red squares. It can be observed that τ_9 and τ_{10} did not form in these diffusion couples. However, the possibility of a missing phase is a common phenomenon in diffusion couples [23]. Sometimes, the nucleation and growth of a phase are too slow to form a diffusion layer to be detected by SEM. In order to overcome this uncertainty a combined investigation with key sample analysis has been carried out and will be discussed in Section 3.2.

3.1.4. Solid-Liquid Diffusion Couple

Two solid-liquid diffusion couples were used to confirm the existence of the ternary compounds identified in the three prior solid-solid diffusion couples. The diffusion zone in solid-solid diffusion couples 2 and 3 (Figures 5 and 7) is quite localized and restricted to a small region because of a not ideal contact between the faying surfaces of the end members. To improve the contact and obtain continuous diffusion layers Mg block was partly melted on top of two different alloy blocks ($Ni_{78}Y_{22}$

and $Ni_{52}Y_{48}$) in an induction melting furnace to form two diffusion couples. This improved the contact and formed continuous diffusion layers as can be seen in Figures 9 and 10.

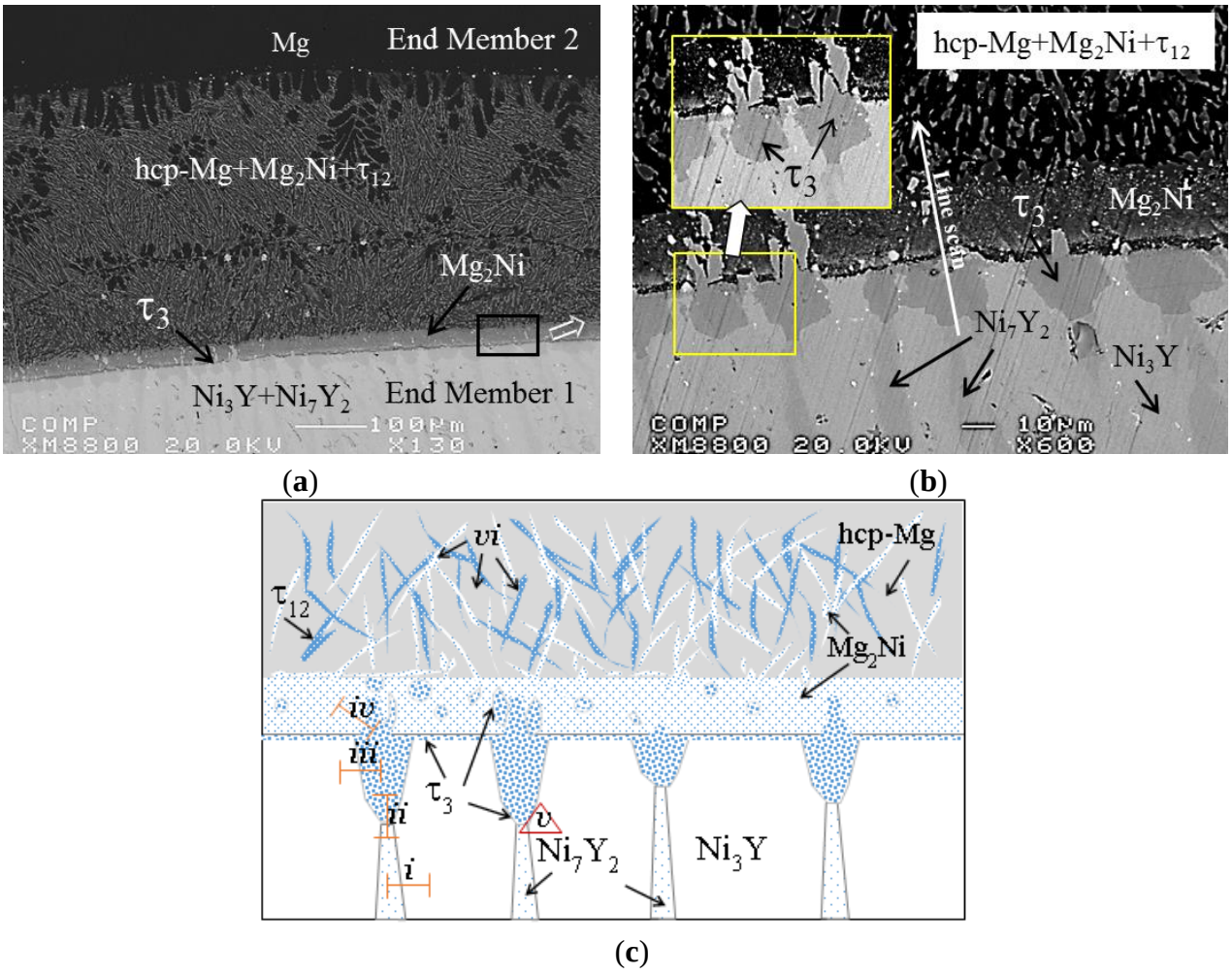

Figure 9. (**a**) BSE images of the solid–liquid diffusion couple-1 (Mg-$Ni_{78}Y_{22}$) annealed at 673 K for 4 weeks; (**b**) Magnified area of interest; (**c**) Schematic representation of the phase relations of the diffusion zone in Figure 9b.

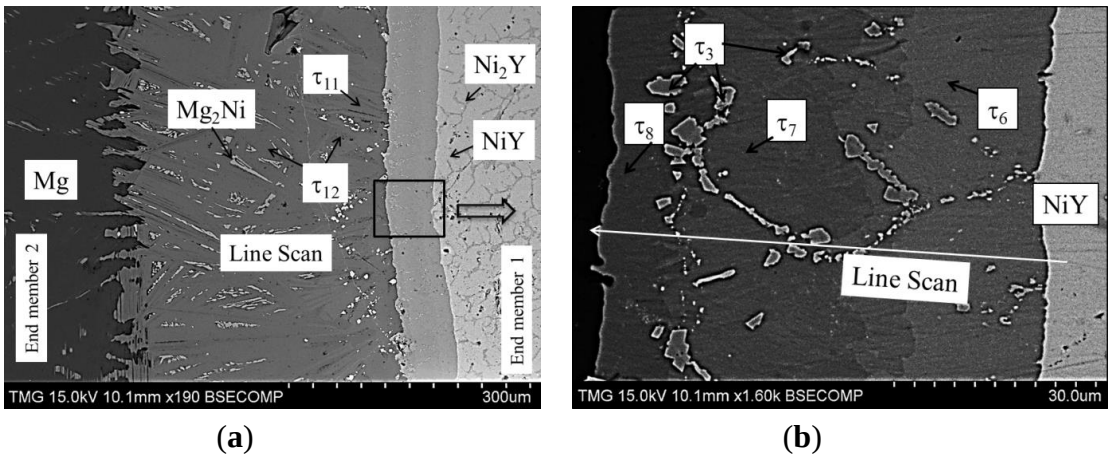

Figure 10. (**a**) BSE images of the solid–liquid diffusion couple-2 (Mg-$Ni_{52}Y_{48}$) annealed at 673 K for 4 weeks; (**b**) Magnified area of interest.

The BSE image of the solid-liquid diffusion couple 1 (Mg-$Ni_{78}Y_{22}$) in Figure 9a shows a three-phase region among hcp-Mg, Mg_2Ni and τ_{12} in contact with pure Mg. Diffusion layers containing three phases are not possible in a ternary system. This area was formed as a result of reaction between molten Mg and solid $Ni_{78}Y_{22}$ end member, generating an alloy in the three-phase region of hcp-Mg + Mg_2Ni + τ_{12}. According to the EDS area scan the average composition of this layer is 84.8/12.6/2.6 Mg/Ni/Y at%. This 3-phase alloy has been considered as the end member of this diffusion couple. The first diffusion layer is τ_3 as can be seen in Figure 9b. The layer is uneven and showed teeth like formation as can be seen in Figure 9b inset. The Gibbs energy of formation of the end member phases: Ni_3Y and Ni_7Y_2 is −34.4 and −33.1 kJ/mole atom, respectively [16]. Since both have comparable energy of formation ΔG, the diffusion kinetics play a more important role for this type of layer formation. In order to explain the phase relations obtained from this diffusion couple a schematic drawing of the diffusion zone is shown in Figure 9c. The following phase relations can be extracted: (i) Ni_3Y + Ni_7Y_2 {end member 1}; (ii) τ_3 + Ni_7Y_2; (iii) τ_3 + Ni_3Y; (iv) τ_3 + Mg_2Ni; (v) τ_3 + Ni_3Y + Ni_7Y_2 and (vi) Mg_2Ni + τ_{12} + hcp-Mg {end member 2}. A line WDS analysis was performed as can be seen in Figure 9b. The composition profile based on the WDS scan is shown in Figure 11. The homogeneity range of τ_3 was found from 14.5 to 19.3 at% Mg with a constant amount of about 64 at% Ni. The solubility limit of this compound was confirmed using key samples and discussed in Section 3.2. Also, the maximum solubility of Y in Mg_2Ni was found to be about 3.5 at%. No solubility of Y or Ni could be detected in the hcp-Mg phase.

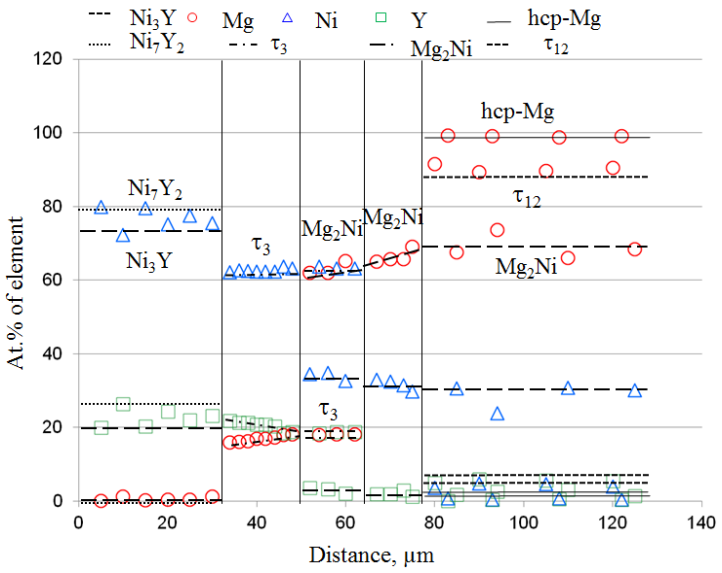

Figure 11. Composition profile of the solid-liquid diffusion couple-1 along the line scan shown in Figure 9b.

The 2nd solid-liquid diffusion couple (Mg-$Ni_{52}Y_{48}$) in Figure 10 also indicates reaction between liquid Mg and the end member $Ni_{52}Y_{48}$. It produced an alloy ($Mg_{78.4}Ni_{15.5}Y_{6.1}$) containing τ_{12} and Mg_2Ni. This alloy is considered as an end member of this diffusion couple. Four diffusion layers formed after annealing and a line WDS scan was carried out through them as can be seen in Figure 10b. The composition profile and diffusion path deduced from the line scan is shown in Figure 12a,b. Three intermetallic compounds τ_6 (~32.0/31.5/36.5 Mg/Ni/Y at%), τ_7 (~42.1/26.2/31.7

Mg/Ni/Y at%) and τ_8 (~48.3/23.5/28.1 Mg/Ni/Y at%) are identified in the first three layers as can be seen in Figure 12a. In between τ_6 and τ_7 another layer can be seen which is found to have less Mg concentration (~39 at%) than τ_7 (42 at%). This indicates that τ_7 may have a narrow solubility range. However, none of the previous diffusion couples showed any solubility of τ_7. Hence, this solubility was not considered while constructing the isothermal section. Also, in all of these layers small precipitates of another phase can be seen. Spot WDS analysis revealed this as τ_3. This means that τ_3 is in equilibrium with all of the ternary compounds in this diffusion couple. This is in agreement with the previous diffusion couples. The fourth diffusion layer is a two-phase region between τ_{11} and τ_{12}. After this the diffusion terminates in the two phase region of Mg_2Ni and τ_{12}.

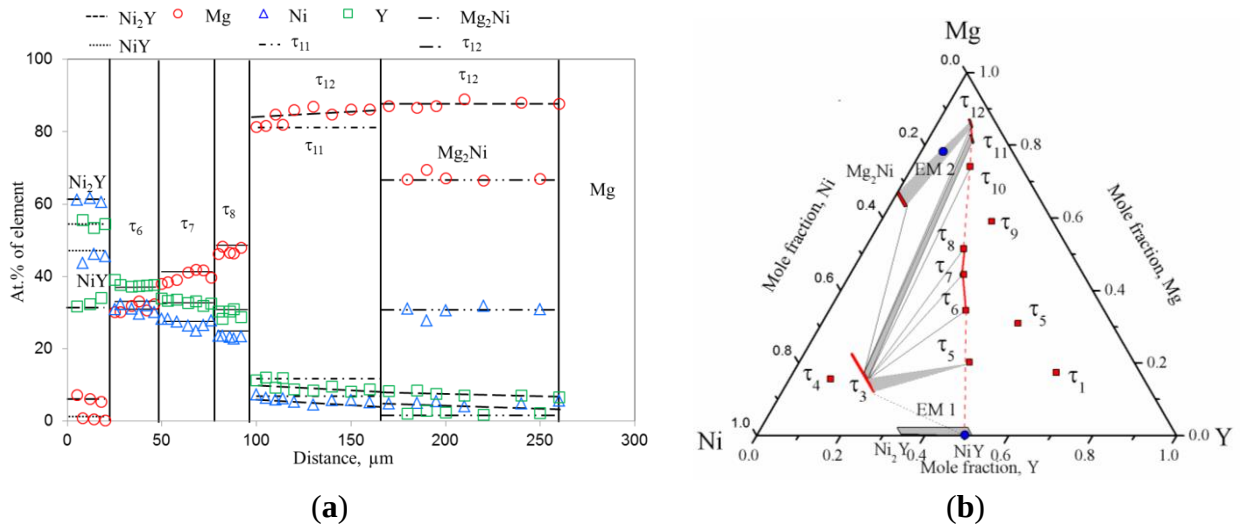

(**a**) (**b**)

Figure 12. (**a**) Composition profile of the solid–liquid diffusion couple-2 along the line scan shown in Figure 10b; (**b**) Extracted phase equilibria based on the solid-liquid diffusion couple-2 projected on the Mg-Ni-Y Gibbs triangle. Dotted lines indicate expected phase equilibria which are not recognized in this DC.

3.2. Isothermal Section based on Diffusion Couples and Key Sample Analysis

In addition to the diffusion couples 32 key alloys were studied in order to construct the isothermal section at 673 K. The BSE images of selected key alloys are shown in Figure 13. The WDS analysis of all the key samples was performed, the samples were grouped based on the phase analysis and are discussed accordingly. The occurrence of twelve ternary compounds (τ_1–τ_{12}) in the Mg-Ni-Y system was confirmed. Among these only two, τ_3 and τ_4 were reported in the literature [12–15]. Based on the current analysis, approximate composition of all the compounds was obtained. The composition and homogeneity range of these ternary compounds are listed in Table 1. The ternary solubility of the binary compounds was also determined. The maximum Ni solubility in MgY(γ), Mg_2Y(δ) and $Mg_{24}Y_5$(ε) was found to be ~1.0 at% Ni. Among the Ni-Y compounds, $Ni_{17}Y_2$ and NiY dissolved about 3.5 and 1.3 at% Mg. The solubility of Mg in Ni_3Y, Ni_4Y and NiY_3 is negligible (~0.5 ± 1 at% Mg). Both, Mg_2Ni and $MgNi_2$ were found to dissolve about 4.0 at% Y.

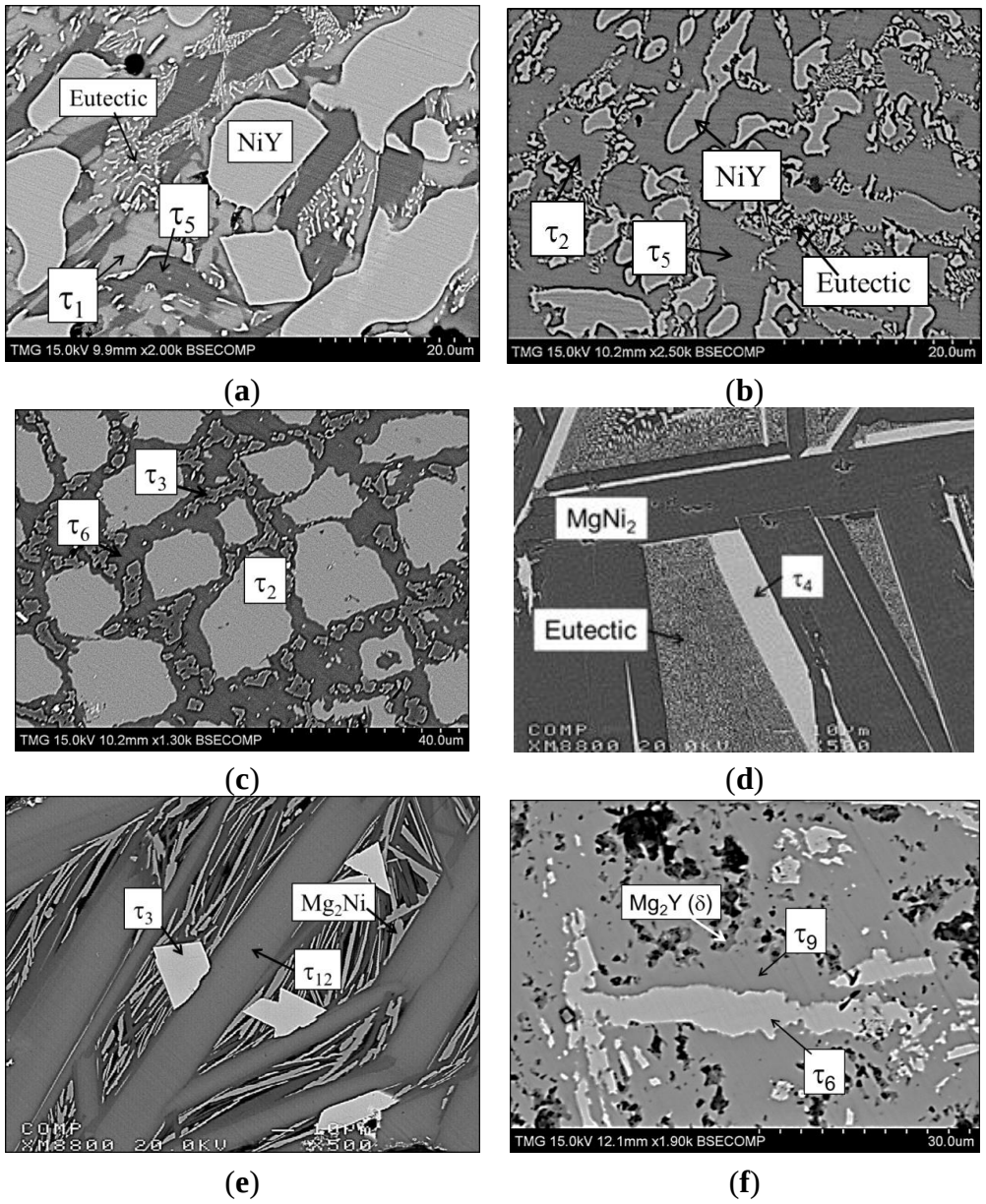

Figure 13. BSE image of (**a**) sample 1 (19.5/29.5/51.0 Mg/Ni/Y at%); (**b**) sample 9 (25.0/30.3/44.7 Mg/Ni/Y at%); (**c**) sample 11 (26.0/38.2/35.8 Mg/Ni/Y at%); (**d**) Sample 18 (28.7/69.1/2.2 Mg/Ni/Y at%); (**e**) sample 25 (78.2/15.5/6.3 Mg/Ni/Y at%); (**f**) sample 30 (54.0/15.9/30.1 Mg/Ni/Y at%).

The presence of the ternary compound τ_1 and the phase relationship in the Y-rich portion of the phase diagram were confirmed by the analysis of eight key samples 1–8. The actual composition of the alloys are shown in Figure 2. In all these alloys, τ_1 is positively identified. The WDS analysis listed in Table 2 shows a range of composition (~15–20 at% Mg, ~16–20 at% Ni) of τ_1 suggesting solid solubility. Variation in all the three elements indicates random substitution of atoms. Therefore, a relatively round region has been assigned to demonstrate the solubility range of τ_1. According to the WDS analysis of τ_1 containing alloys (1–8), five three-phase regions were also established: τ_1 + NiY + Ni_2Y_3, τ_1 + NiY_3 + Ni_2Y_3, τ_1 + NiY + τ_5, τ_1 + MgY + τ_5 and τ_1 + NiY_3 + hcp-Y.

Table 1. Ternary intermetallic compounds in the Mg-Ni-Y system.

Phase	Crystal Structure	Lattice Parameter (nm)		Homogeneity Range	Ref.
		a	*c*		
τ_1-$MgNiY_4$	Gd_4RhIn	1.3666		15–20 at% Mg 16–20 at% Ni	This work
τ_2-$MgNi_2Y_2$	Mo_2FeB_2	0.7395(9)	0.3736(3)		This work
τ_3-$MgNi_4Y$	$MgCu_4Sn$	0.71853		11–23 at% Mg ~66.6 at% Ni	This work
τ_4-Mg_2Ni_9Y	Mg_2Ni_9La	0.48666(5)	2.37733(5)		[12]
τ_5-$Mg_{29}Ni_{20}Y_{42}$	Unknown				This work
τ_6-MgNiY	Unknown				This work
τ_7-$Mg_8Ni_5Y_5$	Unknown				This work
τ_8-Mg_2NiY	Unknown				This work
τ_9-$Mg_{57}Ni_{18}Y_{25}$	Unknown				This work
τ_{10}-Mg_6NiY	Unknown				This work
τ_{11}-Mg_9NiY	Unknown			85.6–89.0 at% Mg at%Ni/at%Y ≅ 1	This work
τ_{12}-$Mg_{15}NiY$	Unknown			81.6–85.0 at% Mg at%Ni/at%Y ≅ 1	This work

Table 2. Wave dispersive X-ray spectrometer (WDS) data of the samples 1–8 annealed at 673 K.

Actual Composition				Identified Phases			
No.	at%			Name	Composition by WDS		
	Mg	Ni	Y		Mg	Ni	Y
1	19.5	29.5	51.0	τ_1	20.9	16.6	62.5
				τ_5	33.6	21.9	44.5
				NiY	0.9	48.9	50.2
2	18.5	22.4	59.1	τ_1	20.1	17.3	62.6
				τ_5	31.7	21.6	46.7
				NiY	0.4	48.7	50.9
3	13.1	26.7	60.2	τ_1	16.4	20.3	63.3
				Eutectic	12.96	29.1	58.0
4	4.8	28.3	66.9	τ_1	16.4	21.3	62.3
				NiY_3	0.9	24.9	74.2
				NiY	0.4	48.8	50.8
5	3.9	23.6	72.5	τ_1	14.7	22.1	63.2
				NiY_3	0.7	25.5	73.8
6	5.9	20.9	73.2	τ_1	16.2	18.6	65.2
				NiY_3	1.2	24.3	74.5
7	8.6	16.5	74.9	τ_1	17.2	16.5	66.2
				NiY_3	0.9	24.4	74.7
				Y-hcp	0.7	0.8	98.5
8	37.0	15.0	48.0	MgY(γ)	51.5	1.6	46.9
				τ_1	26.3	15.6	58.1
				τ_5	32.8	21.4	45.8

Hara *et al.* [7] in their hydrogen storage work on the Mg-Ni-Y system, reported an unknown phase of composition $MgNiY_3$. They reported that this compound plays a role as a catalyst for the adsorption of hydrogen. However, they could not identify the crystal structure of this compound. The composition of this compound ($MgNiY_3$) is very close to the single phase region of τ_1. Hence, it is likely that Hara *et al.* [7] were actually detecting τ_1 ($MgNiY_4$).

The crystallographic information of τ_1 was determined in this work. This was done by comparing XRD patterns of several τ_1 containing alloys (KS# 1–8) with similar structure type compounds from Pearson crystal structure database [27]. It was found that the XRD pattern of Gd_4RhIn was very similar to that of τ_1. Tappe *et al.* [28] reported several rare earth containing compounds with this prototype. Therefore, the crystallographic data of Gd_4RhIn was taken as the starting value for the Rietveld structural refinement of τ_1 in the present work. Using this strategy the lattice parameter of τ_1 was determined as: a = 1.3666 nm. The refined crystal structure data and atomic positions of τ_1 are listed in Tables 3 and 4. Also, the unit cell is shown in Figure 14a. The XRD pattern of sample 2, shown in Figure 15, positively identifies τ_1 and NiY. The SEM analysis of this alloy as listed in Table 2 showed three phases, τ_1 + NiY + τ_5. Therefore it can be said that the unknown peaks in the XRD pattern belong to τ_5. Since the crystal structure of τ_5 is unknown these peaks are labeled by a question mark (?). The statistically expected values R_e (12.6), weighted summation of residuals of the least squared fit R_{wp} (24.9) and goodness of fit s (3.9) were used to judge the degree of refinement in the Rietveld analysis. Due to the unknown peaks of τ_5, a better statistical fit was not possible.

Table 3. The crystal structure data of τ_1 and τ_2.

Compound	**$MgNiY_4$ (τ_1)**			**$MgNi_2Y_2$ (τ_2)**		
Structure	Cubic			Tetragonal		
Prototype	Gd_4RhIn			Mo_2FeB_2		
Space group	$F\bar{4}3m$ (216)			P4/mbm (127)		
Lattice parameter (nm)	*a*			*a*		*c*
	1.3666(0)			0.7395(9)		0.3736(3)
Angles	α	β	γ	α	β	γ
	90 °	90 °	90 °	90 °	90 °	90 °
Atoms in unit cell	96			10		

Table 4. Atoms position in the unit cell of τ_1 and τ_2.

Atom	**Wyckoff Position**	***x***	***y***	***z***
	$MgNiY_4$ (τ_1)			
Mg	16e	0.080	0.080	0.080
Ni	16e	0.640	0.640	0.640
Y1	24g	0.560	0.250	0.250
Y2	24f	0.310	0	0
Y3	16e	0.153	0.153	0.153
	$MgNi_2Y_2$ (τ_2)			
Mg	2a (12)	0	0	0
Ni	4g (9)	0.6216	0.1216	0
Y	4h (17)	0.1716	0.6716	0.5000

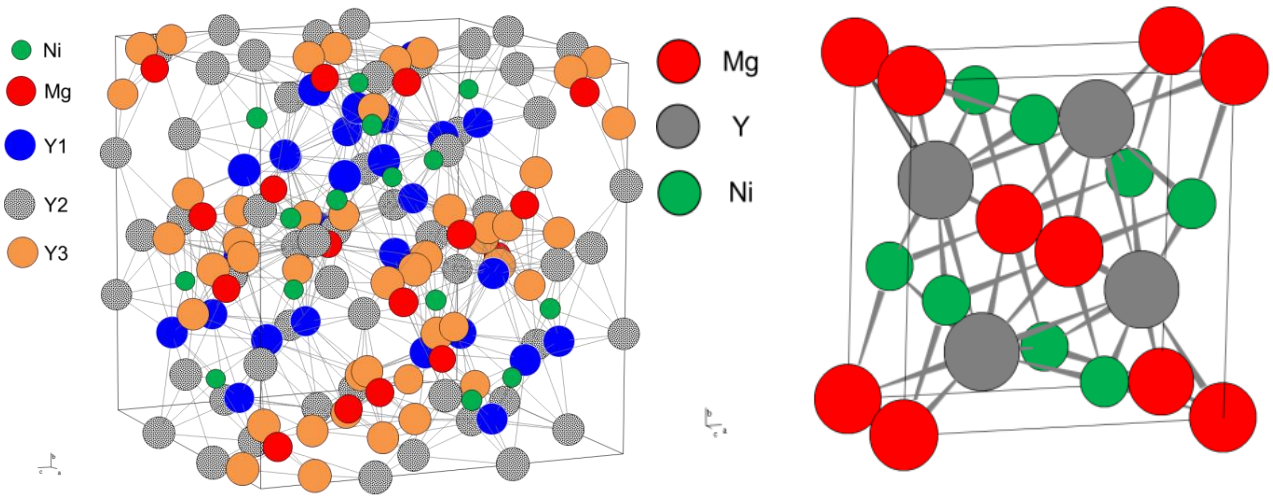

Figure 14. Unit cell for (**a**) τ_1 and (**b**) τ_2.

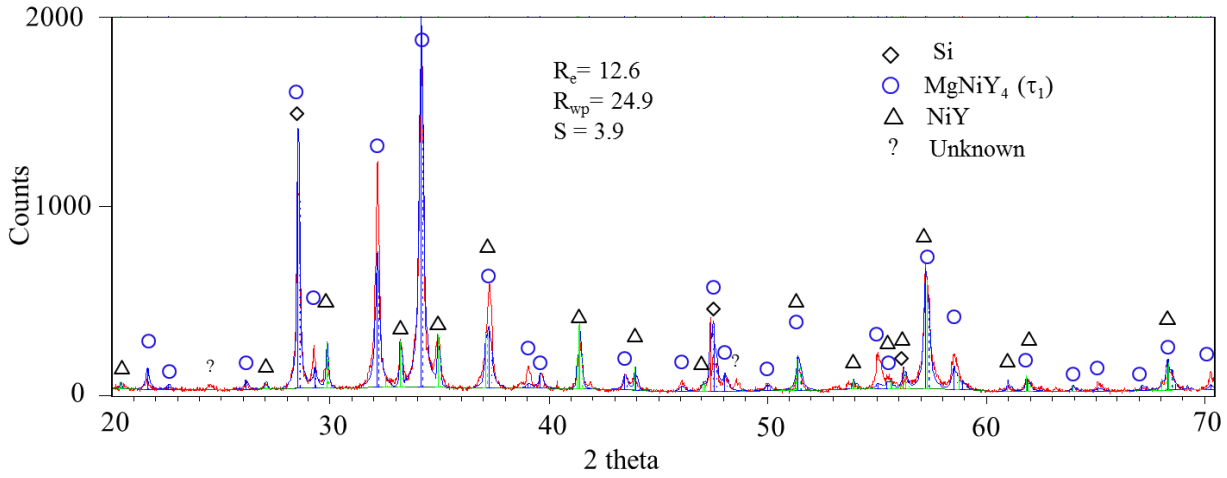

Figure 15. X-ray diffraction (XRD) pattern for sample 2 (18.5/22.4/59.1 Mg/Ni/Y at%).

The ternary compound, τ_2 was not observed in any of the diffusion couples. Therefore more effort was dedicated towards confirming its presence. Five key alloys (9–13) were prepared near this compound. τ_2 was found to exist in all of them. According to the WDS analysis in Table 5, the composition of this compound is 20/40/40 Mg/Ni/Y at%. Based on this, the $MgNi_2Y_2$ formula was assigned to it. These key alloys also demonstrated the occurrence of three 3-phase regions, $\tau_2 + \tau_3 + NiY$, $\tau_2 + \tau_5 + NiY$ and $\tau_2 + \tau_3 + \tau_6$.

The crystallographic information of τ_2 was determined in the present work in a similar approach to that of τ_1 by comparing the XRD patterns of several alloys containing this phase with similar structure type compounds from the Pearson crystal structure database [27]. It was found that τ_2 has Mo_2FeB_2 prototype and the lattice parameters were determined as a = 0.7395(9) nm and c = 0.3736(3) nm. The crystal structure data and atoms position within the unit cell are listed in Tables 3 and 4. Also, the unit cell of τ_2 is shown in Figure 14b.

Table 5. WDS data of the samples 19–26 annealed at 673 K.

No.	Actual Composition (at%)			Identified Phases			
				Name	Composition by WDS		
	Mg	Ni	Y		Mg	Ni	Y
9	25.0	30.3	44.7	τ_2	20.9	37.9	41.2
				τ_5	35.0	21.5	43.5
				NiY	0.3	49.2	50.5
10	28.0	36.8	35.2	τ_2	22.4	39.3	38.3
				τ_3	16.3	64.2	19.5
				τ_6	35.9	32.7	31.4
11	26.0	38.2	35.8	τ_2	21.4	39.2	39.4
				τ_3	16.4	64.0	19.6
				τ_6	35.6	32.3	32.1
12	20.0	50.8	29.2	τ_2	19.7	40.5	39.8
				τ_3	11.8	66.5	21.7
				τ_6	32.2	34.3	33.5
13	8.4	58.6	33.0	NiY	1.3	49.6	49.1
				τ_2	21.2	39.3	39.5
				τ_3	18.0	66.5	15.5

XRD patterns of key alloys 10, 11 and 12 are shown in Figure 16a–c. τ_2 was positively identified in all of them. The unknown phase in these XRD patterns belongs to τ_6. Another ternary compound, τ_3 was also positively identified in these XRD patterns. This compound was first reported by Kadir *et al.* [14]. They reported $SnMgCu_4$ prototype with lattice parameter of 0.71853 nm. This compound was found in several alloys (10–13, 16, 19–25) in the current work. According to the WDS analysis in Tables 5 and 6, τ_3 has solubility from ~11 to 23 at% Mg with constant 66.67 at% Ni. The variation of lattice parameter of τ_3 was also observed in the Rietveld analysis performed on the XRD patterns of four key alloys (5, 9, 10 and 11). The change in lattice parameter, "*a*" of τ_3 with Mg concentration is presented in Figure 17. The atomic radius of Mg (145 pm) is less than that of Y (212 pm). According to Vegard's law, the decrease of size of any atom or ion in a crystal leads directly to the proportional decrease of lattice constants. Hence the lattice parameter "*a*" decreases with the increase of Mg concentration. It reflects substitutional solid solution for τ_3 where Mg replaces Y atoms.

τ_4 (Mg_2Ni_9Y) was identified in sample 17 (11.0/78.9/10.1 Mg/Ni/Y at%) and sample 18 (28.7/69.1/2.2 Mg/Ni/Y at%). Kadir *et al.* Reference [12] reported a hexagonal structure for τ_4, which is iso-structure of $LaMg_2Ni_9$. Two different plate-like structures can be seen in the BSE image of sample 18 in Figure 13d. These were identified as $MgNi_2$ and τ_4.

The intermetallic compound, τ_5 was found in samples 1, 2, 8, 9 and 27–29. Based on the WDS analysis of these alloys in Tables 5 and 7, the approximate composition of τ_5 was determined as 33.8/21.5/44.7 Mg/Ni/Y at%. The BSE image of sample 9 (25.0/30.3/44.7 Mg/Ni/Y at%) in Figure 13b clearly shows τ_5 which is in equilibrium with τ_2 and NiY. The crystal structure of τ_5 is not known. Determining the crystal structure of τ_5 in the same approach as for τ_1 and τ_2 was not successful because a crystallographic prototype has not been found yet.

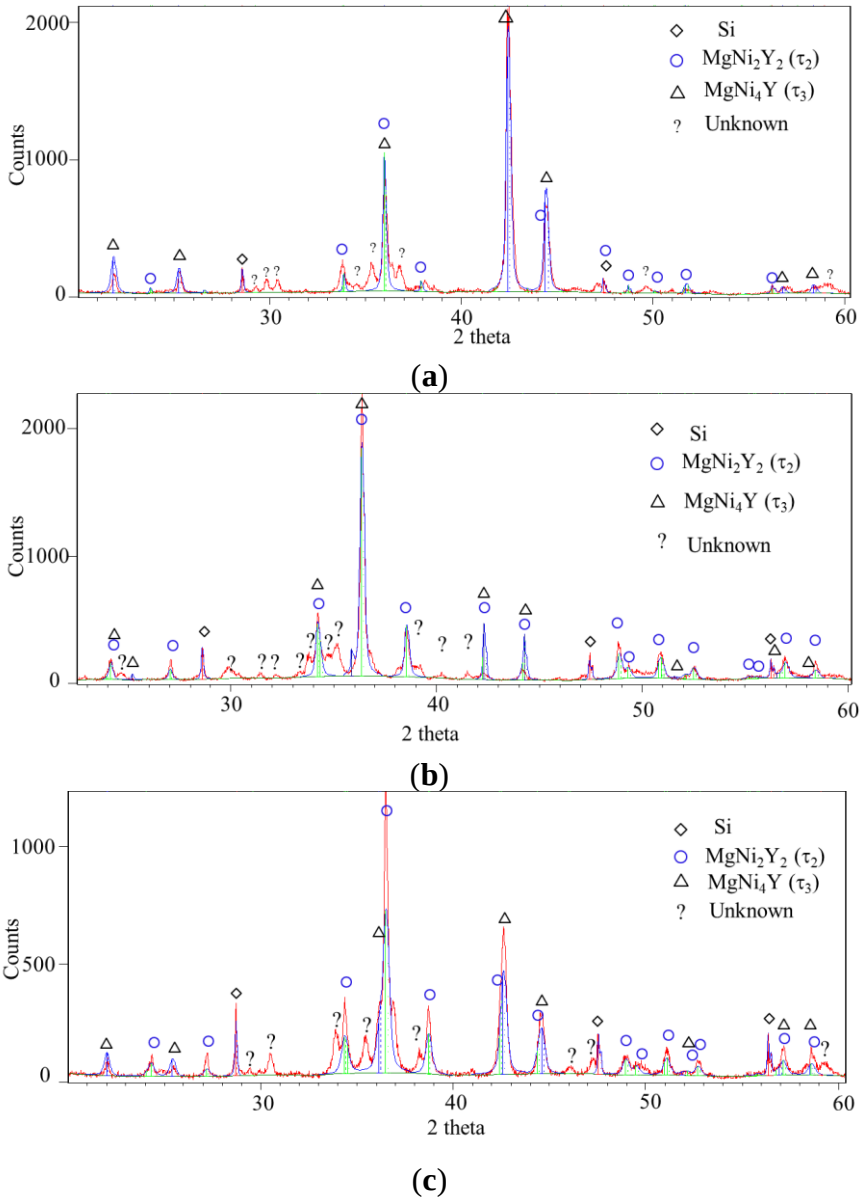

Figure 16. XRD patterns for (**a**) Sample 10 (20.0/50.8/29.2 Mg/Ni/Y at%); (**b**) Sample 11 (26.0/38.2/35.8 Mg/Ni/Y at%); (**c**) sample 12 (28.0/36.8/35.2 Mg/Ni/Y at%).

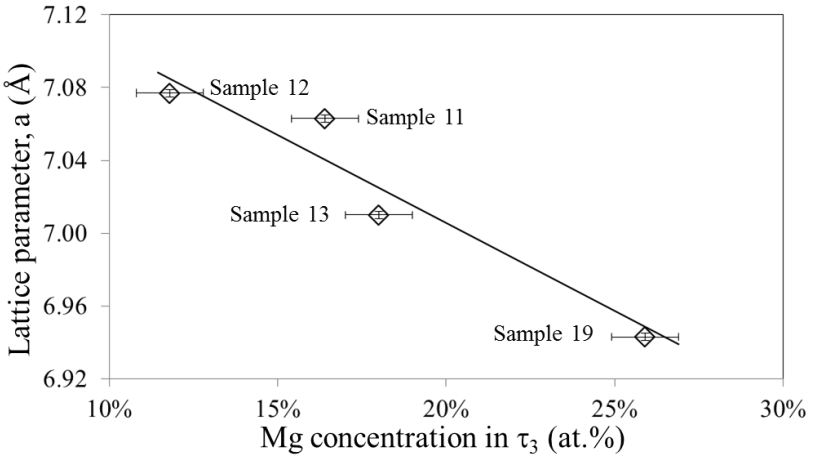

Figure 17. Variation of lattice parameter of τ_3.

Table 6. WDS data of the samples 14–26 annealed at 673 K.

No.	Actual Composition at%			Identified Phases			
				Name	Composition by WDS		
	Mg	Ni	Y		Mg	Ni	Y
14	1.5	63.4	35.1	Ni_2Y	0.7	63.1	36.2
				NiY	0.5	46.7	52.8
15	3.3	80.5	16.2	Ni_5Y	0.7	82.9	16.4
				τ_4	15.5	74.7	9.8
16	3.7	77.3	19.0	Ni_5Y	0.4	82.9	16.7
				τ_3	9.8	66.9	23.3
				Ni_4Y	1.3	78.8	19.9
17	11.0	78.9	10.1	$Ni_{17}Y_2$	3.5	84.9	11.6
				τ_4	17.6	75.6	6.8
18	28.7	69.1	2.2	$MgNi_2$	31.3	66.8	1.8
				τ_4	16.5	75.4	8.1
19	36.2	59.9	3.9	Mg_2Ni	67.2	32.5	0.3
				τ_3	25.9	64.9	9.2
				$MgNi_2$	31.4	64.3	4.3
20	27.2	59.9	12.9	Mg_2Ni	67.2	32.5	0.3
				τ_3	22.7	64.9	12.3
21	24.5	52.4	23.1	τ_3	15.1	64.7	20.2
				τ_7	45.9	27.1	27.0
				τ_8	51.2	24.5	24.3
22 *	37.2	36.3	26.5	τ_3	15.6	65.1	19.3
				τ_6	34.6	31.7	33.7
				τ_8	51.2	24.4	24.4
				τ_{10}	74.1	13.0	12.9
				τ_{11}	82.5	8.6	8.9
23 *	54.1	24.0	21.9	τ_3	17.8	64.1	18.1
				τ_8	52.3	24.3	23.4
				τ_{10}	74.5	12.8	12.7
				τ_{11}	84.5	7.6	7.9
24	55.5	36.6	7.9	τ_{12}	85.1	6.7	8.2
				Mg_2Ni	65.3	33.8	0.9
				τ_3	17.4	66.8	15.8
25	78.2	15.5	6.3	τ_{12}	85.3	6.3	8.4
				Mg_2Ni	67.5	30.7	1.8
				τ_3	18.8	64.5	16.5
26	84.9	12.9	2.2	hcp-Mg	99.4	0.5	0.1
				τ_{12}	92.0	4.1	3.9
				Mg_2Ni	67.9	30.2	1.9

* The samples indicated with (*) are not in complete equilibrium.

The BSE images of sample 22 (37.2/36.3/26.5 Mg/Ni/Y at%) and sample 29 (51.4/12.3/36.3 Mg/Ni/Y at%) in Figure 18a,b, show the presence of τ_6. This compound was also found in

samples 10–12 and 29. In order to obtain equilibrium, these alloys were annealed for six weeks instead of four. Still complete equilibrium could not be obtained. This is probably due to the peritectic decomposition of some of the compounds. The BSE image of sample 22 in Figure 18a shows several phases; τ_3, τ_6, τ_8, τ_{10}, and τ_{11}. Based on the analysis of samples 22 and 23 and the diffusion couples, it can be concluded that τ_3 is in equilibrium with all the compounds in the vicinity of the Mg-NiY line.

Although not in complete equilibrium, a three-phase relation among $Mg_2Y(\delta)$, τ_5 and τ_6 can be identified in sample 29 (51.4/12.3/36.3 Mg/Ni/Y at%) in Figure 18b. It is observed that τ_2 (white-square shape) always remains within τ_6 and will probably transfer to τ_6 after a much longer annealing time. This indicates a three-phase region: $Mg_2Y(\delta) + \tau_5 + \tau_6$. The colors of τ_5 and τ_6 are very close because of their similar composition. This makes it difficult to recognize these two phases in the BSE image.

The ternary compounds τ_7 and τ_8 were found in sample 21 (24.6/52.4/23.0 Mg/Ni/Y at%). τ_8 was also identified in samples 22 and 23. The WDS analysis of these alloys is summarized in Table 6. Their presence was also confirmed in three diffusion couples (DC{SS} 2, 3 and DC{SL} 2) as shown earlier in Figures 5, 7 and 10, respectively.

Table 7. WDS data of the samples 27–32 annealed at 673 K.

Actual Composition				**Identified Phases**			
No.	**at%**			**Name**	**Composition by WDS**		
	Mg	**Ni**	**Y**		**Mg**	**Ni**	**Y**
27	38.5	14.7	46.8	MgY(γ)	49.6	1.1	49.3
				τ_5	34.1	21.5	44.4
				$Mg_2Y(\delta)$	-	-	-
28	49.9	8.0	42.1	$Mg_2Y(\delta)$	68.6	0.4	31.0
				MgY(γ)	53.4	0.8	45.8
				τ_5	34.1	21.1	44.8
29 *	51.4	12.3	36.3	τ_2	21.4	37.5	41.1
				τ_5	35.7	21.6	42.7
				τ_6	36.2	30.8	33.0
				$Mg_2Y(\delta)$	71.7	0.8	27.5
30	54.0	15.9	30.1	τ_6	35.1	32.4	32.5
				τ_9	56.7	16.5	26.8
				$Mg_2Y(\delta)$	69.1	1.5	29.4
31	69.1	9.4	21.5	τ_9	57.5	16.4	26.1
				τ_{10}	67.0	14.1	18.9
				$Mg_2Y(\delta)$	72.6	1.4	26.0
32	72.0	6.3	21.7	τ_{10}	67.1	12.3	20.6
				$Mg_2Y(\delta)$	73.5	1.1	25.4

* The sample indicated with (*) are not in complete equilibrium.

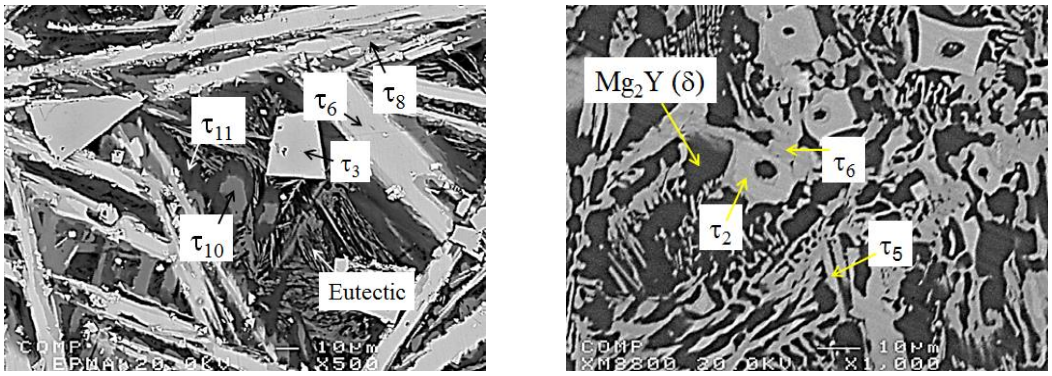

(**a**) (**b**)

Figure 18. BSE image of (**a**) sample 22 (37.2/36.3/26.5 Mg/Ni/Y at%); (**b**) Sample 29 (51.4/12.3/36.3 Mg/Ni/Y at%).

The BSE image of sample 30 (54.0/15.9/30.1 Mg/Ni/Y at%) in Figure 13f shows a three-phase equilibrium among $Mg_2Y(\delta)$, τ_6 and τ_9. The white flakes and the grey matrix in the microstructure were identified as τ_6 and τ_9, respectively. $Mg_2Y(\delta)$ was found as fine precipitates in the grey matrix. According to the WDS analysis of sample 30 in Table 7, the composition of the ternary compound τ_9 is 56.7/16.5/26.8 Mg/Ni/Y at%. This compound was also observed in the solid-solid diffusion couple 1 in Figure 3 with slightly different composition 59.1/16.5/24.3 Mg/Ni/Y at%. The WDS analysis of sample 31 (69.1/9.4/21.5 Mg/Ni/Y at%) in Table 7, identified this compound, τ_9, as 57.5/16.4/26.1 Mg/Ni/Y at%, which is closer to the diffusion couple analysis. Therefore, it was decided to use the composition obtained by the diffusion couple analysis since it is generally more accurate.

The WDS analysis of sample 31 (69.1/9.4/21.5 Mg/Ni/Y at%) and sample 32 (72.0/6.3/21.7 Mg/Ni/Y at%) in Table 7, showed a three-phase, $Mg_2Y(\delta) + \tau_9 + \tau_{10}$, and a two-phase, $Mg_2Y(\delta) + \tau_{10}$ equilibria. Both of these alloys confirmed the existence of the ternary compound τ_{10} with an average composition 66.4/12.7/20.9 Mg/Ni/Y at%. However, the solid-solid diffusion couple 2 shown in Figure 5 revealed the composition as 74.7/12.9/12.4 Mg/Ni/Y at%. The compositional variation is probably due to a linear solubility of τ_{10} from ~66.4 at% (sample 31 and 32) to 74.7 at% Mg at constant Ni of ~12.7 at%. The diffusion layer for τ_{10} in the solid-solid diffusion couple 2, is only 6 μm which was not wide enough for detecting the solubility. Therefore, the solubility of τ_{10} could not be confirmed.

Two ternary compounds τ_{11} and τ_{12} in the Mg-rich corner of the Mg-Ni-Y phase diagram were identified in this work. τ_{11} was found in key samples 22 (37.2/36.3/26.5 Mg/Ni/Y at%) and 23 (53.0/25.1/21.9 Mg/Ni/Y at%). Also, solid-solid diffusion couples 2 and 3 in Figures 5 and 7, showed the presence of τ_{11}. It was found that τ_{11} has a solid solubility, which extends from ~82 to 85 at% Mg. τ_{12} was found in all three solid-solid diffusion couples as well as in key samples 24 (55.5/36.6/7.9 Mg/Ni/Y at%), 25 (78.2/15.5/6.3 Mg/Ni/Y at%) and 26 (84.9/12.9/2.2 Mg/Ni/Y at%). According to the WDS analysis, τ_{12} has a solubility range, which extends from ~85 to 89 at% Mg.

Based on the current results, an isothermal section of the Mg-Ni-Y system at 673 K was constructed as shown in Figure 19. The dotted lines in the isothermal section show the tentative phase relations, as these could not be confirmed experimentally due to very sluggish kinetics.

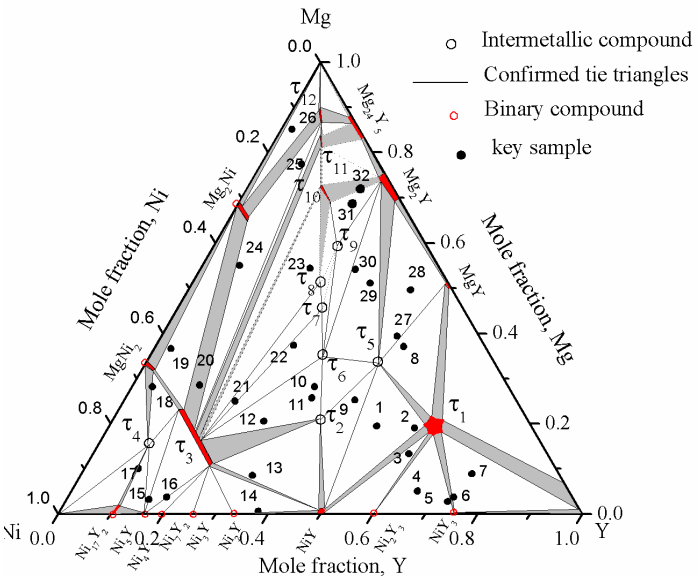

Figure 19. Isothermal section of the Mg-Ni-Y system at 673 K for the whole composition.

4. Summary

The isothermal section of the Mg-Ni-Y phase diagram at 673 K for the whole composition range was constructed using diffusion couples and key samples for the first time. The homogeneity ranges of ternary and binary compounds were determined and the phase relations among them were established using WDS and XRD studies. Ten new ternary compounds (τ_1, τ_2, τ_5–τ_{12}) were discovered in this system. The existence of two ternary compounds τ_3 and τ_4 were also confirmed. Ternary solubility of five of the ternary compounds, τ_1, τ_3, τ_{10}, τ_{11}, and τ_{12} at 673 K was determined and the rest were assumed stoichiometric compounds. Crystal structures of τ_1 (Gd_4RhIn) and τ_2 (Mo_2FeB_2) were determined. The lattice parameter of τ_1 is a = 1.3666 nm, and τ_2 is a = 0.7395(9) nm and c = 0.3736(3) nm. τ_3 is the most stable ternary compound which has solid solutions from 11 to 23 at% Mg, where Mg substitutes Y at constant 66% Ni. All the intermetallics along the Mg-NiY section are in equilibrium with τ_3.

Acknowledgments

This research was carried out with the support of NSERC Alexander Graham Bell Canada Graduate Scholarship (NSERC CGS). The authors wish to express their appreciation for this support.

Author Contributions

Mamoun Medraj initiated the project. Mohammad Mezbahul-Islam and Mamoun Medraj designed the experiments. Mohammad Mezbahul-Islam performed the experiments. Mohammad Mezbahul-Islam, Dmytro Kevorkov and Mamoun Medraj interpreted the results. Mohammad Mezbahul-Islam wrote the manuscript with the suggestions of Dmytro Kevorkov and Mamoun Medraj. Mamoun Medraj revised the manuscript.

Conflicts of Interest

The authors declare no conflict of interest.

References

1. Kim, S.G.; Inoue, A.; Masumoto, T. High mechanical strengths of magnesium-nickel-yttrium and magnesium-copper-yttrium amorphous alloys with significant supercooled liquid region. *Mater. Trans. Jpn. Inst. Metals Mater.* **1990**, *31*, 929–934.
2. Puech, S.; Blandin, J.-J.; Soubeyroux, J.-L. Mg based bulk metallic glasses with high mechanical strength and large viscoplastic forming capacity. *Adv. Eng. Mater.* **2007**, *9*, 764–768.
3. Katz-Demyanetz, A.; Rosenson, H.; Koren, Z.; Regev, M. Bulk metallic glass formation in the Mg-Cu-Y system. *Mater. Sci. Technol.* **2009**, *25*, 1227–1233.
4. Inoue, A.; Masumoto, T. Mg-based amorphous alloys. *Mater. Sci. Eng. A* **1993**, *173*, 1–8.
5. Zhao, X.; Ma, L. Recent progress in hydrogen storage alloys for nickel/metal hydride secondary batteries. *Int. J. Hydrogen Energy* **2009**, *34*, 4788–4796.
6. Abrosimova, G.E. Formation of the metastable phase upon crystallization of light amorphous Mg-Ni-Y alloys. *Phys. Solid State* **2002**, *44*, 204–209.
7. Hara, M.; Morozumi, S.; Watanabe, K. Effect of a magnesium depletion on the Mg-Ni-Y alloy hydrogen absorption properties. *J. Alloys Compd.* **2006**, *414*, 207–214.
8. Orimo, S.; Züttel, A.; Ikeda, K.; Saruki, S.; Fukunaga, T.; Fujii, H.; Schlapbach, L. Hydriding properties of the MgNi-based systems. *J. Alloys Compd.* **1999**, *293–295*, 437–442.
9. Savyak, M.; Hirnyj, S.; Bauer, H.D.; Uhlemann, M.; Eckert, J.; Schultz, L.; Gebert, A. Electrochemical hydrogenation of $Mg_{65}Cu_{25}Y10$ metallic glass. *J. Alloys Compd.* **2004**, *364*, 229–237.
10. Du, Y.; Xu, L.; Shen, Y.; Zhuang, W.; Zhang, S.; Chen, G. Hydrogen absorption/desorption behavior of $Mg_{50}La_{20}Ni_{30}$ bulk metallic glass. *Int. J. Hydrogen Energy* **2013**, *38*, 4670–4674.
11. Yao, Q.; Zhou, H.; Wang, Z. The isothermal section of the phase diagram of the ternary system Y-Mg-Ni at 673 K in the region 50–100 at% Ni. *J. Alloys Compd.* **2006**, *421*, 117–119.
12. Kadir, K.; Sakai, T.; Uehara, I. Structural investigation and hydrogen capacity of YMg_2Ni_9 and $(Y_{0.5}Ca_{0.5})(MgCa)Ni_9$: New phases in the AB_2C_9 system isostructural with $LaMg_2Ni_9$. *J. Alloys Compd.* **1999**, *287*, 264–270.
13. Kadir, K.; Sakai, T.; Uehara, I. Synthesis and structure determination of a new series of hydrogen storage alloys; RMg_2Ni_9 (R = La, Ce, Pr, Nd, Sm and Gd) built from $mgni_2$ laves-type layers alternating with AB_5 layers. *J. Alloys Compd.* **1997**, *257*, 115–121.
14. Kadir, K.; Noreus, D.; Yamashita, I. Structural determination of AMgNi4 (where A = Ca, La, Ce, Pr, Nd and Y) in the AuBe5 type structure. *J. Alloys Compd.* **2002**, *345*, 140–143.
15. Aono, K.; Orimo, S.; Fujii, H. Structural and hydriding properties of $MgYNi_4$: A new intermetallic compound with C15b-type Laves phase structure. *J. Alloys Compd.* **2000**, *309*, L1–L4.
16. Mezbahul-Islam, M.; Medraj, M. A critical thermodynamic assessment of the Mg-Ni, Ni-Y binary and Mg-Ni-Y ternary systems. *CALPHAD* **2009**, *33*, 478–486.

17. Mezbahul-Islam, M.; Kevorkov, D.; Essadiqi, E.; Medraj, M. Ternary intermetallic compounds across the Mg-NiY line at 673 K. *Mater. Sci. Forum* **2012**, *706–709*, 1134–1139.
18. Wang, Z.; Luo, Q.; Chen, S.; Chou, K.-C.; Li, Q. Experimental investigation and thermodynamic calculation of the Mg–Ni–Y system (Y < 50 at%) at 400 and 500 ℃. *J. Alloys Compd.* **2015**, *649*, 1306–1314.
19. Jiang, M.; Zhang, S.; Bi, Y.; Li, H.; Ren, Y.; Qin, G. Phase equilibria of the long-period stacking ordered phase in the Mg-Ni-Y system. *Intermetallics* **2015**, *57*, 127–132.
20. Zhao, J.-C. A combinatorial approach for structural materials. *Adv. Eng. Mater.* **2001**, *3*, 143–147.
21. Zhao, J.-C. A combinatorial approach for efficient mapping of phase diagrams and properties. *J. Mater. Res.* **2001**, *16*, 1565–1578.
22. Van Loo, F.J.J. Multiphase diffusion in binary and ternary solid-state systems. *Progress Solid State Chem.* **1990**, *20*, 47–99.
23. Kodentsov, A.A.; Bastin, G.F.; van Loo, F.J.J. The diffusion couple technique in phase diagram determination. *J. Alloys Compd.* **2001**, *320*, 207–217.
24. Zhao, J.C.; Jackson, M.R.; Peluso, L.A. Determination of the Nb–Cr–Si phase diagram using diffusion multiples. *Acta Mater.* **2003**, *51*, 6395–6405.
25. Zhao, H.D.; Qin, G.W.; Ren, Y.P.; Pei, W.L.; Chen, D.; Guo, Y. The maximum solubility of Y in α-Mg and composition ranges of $Mg_{24}Y_{5-x}$ and Mg_2Y_{1-x} intermetallic phases in Mg–Y binary system. *J. Alloys Compd.* **2011**, *509*, 627–631.
26. Mezbahul-Islam, M.; Mostafa, A.O.; Medraj, M. Essential magnesium alloys binary phase diagrams and their thermochemical data. *J. Mater.* **2014**, doi:10.1155/2014/704283.
27. Villars, P.; Cenzual, K. *Pearson's Crystal Data—Crystal Structure Database for Inorganic Compounds* [CD-ROM]; ASM International: Materials Park, OH, USA, 2009.
28. Tappe, F.; Schwickert, C.; Linsinger, S.; Poettgen, R. New rare earth-rich aluminides and indides with cubic Gd_4RhIn-type structure. *Monatsh. Chem.* **2011**, *142*, 1087–1095.